


## Aspects of the normal state resistivity of cuprate superconductors

B. Sriram Shastry<sup>1,\*</sup> and Peizhi Mai<sup>2,1</sup>

<sup>1</sup>*Physics Department, University of California, Santa Cruz, California 95064, USA*

<sup>2</sup>*CNMS, Oak Ridge National Laboratory, Oak Ridge, Tennessee 37831-6494, USA*

 (Received 21 November 2019; revised manuscript received 14 January 2020; accepted 11 February 2020; published 13 March 2020)

Planar normal state resistivity data taken from three families of cuprate superconductors are compared with theoretical calculations from the recent extremely correlated Fermi liquid theory (ECFL) [B. S. Shastry, *Phys. Rev. Lett.* **107**, 056403 (2011)]. The two hole-doped cuprate materials LSCO and BSLCO and the electron-doped material LCCO have yielded rich data sets at several densities  $\delta$  and temperatures  $T$ , thereby enabling a systematic comparison with theory. The recent ECFL resistivity calculations for the highly correlated  $t$ - $t'$ - $J$  model by us give the resistivity for a wide set of model parameters [B. S. Shastry and P. Mai, *New J. Phys.* **20**, 013027 (2018); P. Mai and B. S. Shastry, *Phys. Rev. B* **98**, 205106 (2018)]. After using x-ray diffraction and angle-resolved photoemission data to fix parameters appearing in the theoretical resistivity, only one parameter, the magnitude of the hopping  $t$ , remains undetermined. For each data set, the slope of the experimental resistivity at a *single* temperature-density point is sufficient to determine  $t$ , and hence the resistivity on absolute scale at all remaining densities and temperatures. This procedure is shown to give a fair account of the entire data.

DOI: [10.1103/PhysRevB.101.115121](https://doi.org/10.1103/PhysRevB.101.115121)

### I. INTRODUCTION

Understanding the normal state resistivity of high- $T_c$  cuprate superconductors and other strongly correlated materials is a challenging problem. The resistivity reveals the nature of the lowest energy charge excitations and therefore constitutes a relatively simple and yet fundamental probe of matter. In cuprates the different chemical compositions, conditions of preparation, and temperatures and a wide range of electronic densities lead to a complex variety of data sets. These are almost impossible to understand within the standard Fermi liquid theory of metals. Major puzzles are the almost  $T$ -linear planar resistivity of the hole-doped cuprates, the  $T^2$  resistivity of the closely related electron-doped cuprates, and the intermediate behavior at various densities. Indeed one of the larger questions about the cuprates is whether the differing  $T$  dependence of the electron-doped and hole-doped cases can possibly arise from a common physical model. Equally puzzling is the drastic reduction of the observed  $T$  scale of the resistivity variation ( $\sim 100$ – $400$  K) from a bare bandwidth ( $\sim eV$ 's) by a few orders of magnitude for both electron-doped and hole-doped cuprates. This situation has generated an upsurge of often radically new theoretical work on correlated systems in the last three decades, amounting to something like a revolution in condensed matter physics. In this new class of theories the planar resistivity stands at the center [1–14]; its unusual temperature dependence is most often emphasized.

In this work we bring theory face to face with experimental data on resistivity. We focus on the extremely correlated Fermi liquid theory (ECFL) proposed by Shastry [1,15,16], where a detailed and meaningful comparison has become

possible, as explained below. Starting from a microscopic Hamiltonian, the ECFL theory yields the resistivity on an absolute scale with a very few parameters determining the underlying model. The resistivity is calculated starting from the  $t$ - $t'$ - $J$  model [17–19] containing four parameters, of which three parameters can be fixed using ARPES and x-ray crystal structure data; thus only *one* parameter remains undetermined. The theory works in 2 dimensions without introducing any redundant degrees of freedom, and therefore the results can be meaningfully tested against data on a variety of cuprates, including both hole-doped and electron-doped cases.

### II. SUMMARY OF THE ECFL THEORY

A summary of the basic ideas and context of the ECFL theory is provided here; readers familiar with these ideas may skip to the later sections giving the results. The ECFL formalism is applicable in any dimension to doped Mott-Hubbard systems described by the  $t$ - $t'$ - $J$  model [17–19]

$$H = -t \sum_{\langle i,j \rangle} (\tilde{C}_{i\sigma}^\dagger \tilde{C}_{j\sigma} + \text{H.c.}) - t' \sum_{\langle\langle i,j \rangle\rangle} (\tilde{C}_{i\sigma}^\dagger \tilde{C}_{j\sigma} + \text{H.c.}) + J \sum_{\langle i,j \rangle} \left( \tilde{S}_i \cdot \tilde{S}_j - \frac{1}{4} n_i n_j \right), \quad (1)$$

where  $\langle i,j \rangle$  ( $\langle\langle i,j \rangle\rangle$ ) denotes a sum over nearest (next-nearest) neighbors  $i, j$ , the Gutzwiller projector is given by  $P_G = \prod_i (1 - n_{i\uparrow} n_{i\downarrow})$ , the operator  $\tilde{C}_{i\sigma} = P_G C_{i\sigma} P_G$  is the Gutzwiller-projected version of the standard (canonical) fermion operator, and  $\tilde{S}_i$  ( $n_i$ ) the spin (density) operator at site  $i$ . This model is in essence obtained from the Hubbard model by a canonical transformation implementing the large- $U$  limit [17]. The transformation preserves the physics of the strong-coupling Hubbard

\*sriram@physics.ucsc.edu

model at the lowest energies. The large energy scale  $U$  of the Hubbard model is traded for noncanonical anticommutation relations between Gutzwiller-projected electrons in the  $t$ - $t'$ - $J$  model. Standard (Feynman) diagrammatic many-body techniques do not apply to the  $t$ - $J$  model due to the effect of the Gutzwiller projection on the anticommutation relations. For the relevant operators  $\tilde{C}, \tilde{C}^\dagger$  of the model Eq. (1), the canonical fermionic anticommutator  $\{C_{i\sigma_i}, C_{j\sigma_j}^\dagger\} = \delta_{ij}\delta_{\sigma_i\sigma_j}$  is replaced by a noncanonical anticommuting Lie algebra

$$\{\tilde{C}_{i\sigma_i}, \tilde{C}_{j\sigma_j}^\dagger\} = \delta_{ij}(\delta_{\sigma_i\sigma_j} - \sigma_i\sigma_j\tilde{C}_{i\bar{\sigma}_i}^\dagger\tilde{C}_{j\bar{\sigma}_j}), \quad (2)$$

where  $\bar{\sigma}_i = -\sigma_i$ . An immediate resulting problem is that Wick's theorem simplifying products of operators into pairwise contractions is now invalid. Hence a formally exact and systematic Feynman-Dyson series expansion of the Green's functions in a suitable parameter is unavailable. On the other hand, in the Hubbard model with canonical fermions, the Feynman-Dyson series exists but is not controllable since  $U$  the parameter of expansion is very large for strong correlations. In trading the Hubbard model for the  $t$ - $J$  model in the Gutzwiller-projected subspace, we gain the tactical advantage of avoiding accounting for the large energy scale. However this advantage is lost unless we succeed in finding a corresponding formally exact expansion to replace the Feynman-Dyson series. The ECFL formalism solves this problem by replacing the Feynman-Dyson series with an alternate  $\lambda$  series. This series is formally exact and is an expansion of the Green's functions in a parameter  $\lambda$ . This parameter lives in a finite domain  $\lambda \in [0, 1]$ , interpolating between the free Fermi gas at  $\lambda = 0$  and the fully Gutzwiller-projected limiting case  $\lambda = 1$ . One way is to introduce  $\lambda$  as the coefficient of the noncanonical term in the anticommutator Eq. (2). For analogy it is useful to compare Eq. (2) with the contrast between the commutators of canonical bosons and the usual rotation group  $[SU(2)]$  Lie algebra of spin- $S$  particles. One finds [20] that  $\lambda$  plays a parallel role to the inverse spin, in the theory of quantum spin systems, i.e.,  $\lambda \leftrightarrow \frac{1}{2S}$ , where  $S = \frac{1}{2}, 1, \dots$ . For computing the Green's functions, we note the *exact* functional differential equation of the canonical Hubbard model and the  $t$ - $J$  model written in shorthand space-time-spin matrix notation [1,2] as

$$\left(g_0^{-1} - U \frac{\delta}{\delta\mathcal{V}} - UG\right) \cdot G = \delta\mathbb{1}, \quad (3)$$

$$(g_0^{-1} - \lambda\hat{X} - \lambda\hat{Y}_1) \cdot G = \delta(\mathbb{1} - \lambda\gamma), \quad (4)$$

where  $g_0^{-1}$  is the noninteracting Green's function,  $\gamma$  is a local version of  $G$ , and the remaining terms [of a similar character to the 2nd and 3rd terms in Eq. (3)] are detailed in [1,2]. Here Eq. (3) is the functional differential equation for the Hubbard model. By inverting the operator multiplying  $G$  and expanding in  $U$ , one generates the complete Feynman series in powers of  $U$  for the Hubbard model. In Eq. (4)  $\lambda$  is set at unity to obtain the exact equation for the  $t$ - $J$  model. Its iteration of the above type is not straightforward due to the extra time-dependent term on the right-hand side. These are the equations of motion in the presence of a space-time-spin dependent potential  $\mathcal{V}$ , which is set at zero at the end as prescribed in the Schwinger-Tomonaga method of field theory. The fermionic antiperiodic boundary conditions on

$G$  in the imaginary-time variable complete the mathematical statement of the problem. The ECFL formalism converts the noncanonical equation (4) into a pair of equations of the type Eq. (3) by introducing a decomposition of the Green's function  $G = g \cdot \tilde{\mu}$  into auxiliary Green's function  $g$  and a caparison function  $\tilde{\mu}$ . These pieces satisfy the exact equations

$$(g_0^{-1} - \lambda\overline{X} \cdot g \cdot g^{-1} - \lambda\hat{Y}_1) \cdot g = \delta\mathbb{1}, \quad (5)$$

$$\tilde{\mu} = \delta(\mathbb{1} - \lambda\gamma) + \lambda\overline{X} \cdot g \cdot \tilde{\mu}, \quad (6)$$

where the contraction symbol indicates that the functional derivative contained in  $X$  acts on the term at the other end of the symbol, while other terms satisfy matrix product rules. Notice that Eq. (5) looks similar to Eq. (3) with a unit matrix on the right-hand side, and is thus essentially like a canonical Green's function expression. The second equation, Eq. (6), must be solved simultaneously with Eq. (5), since  $\hat{Y}_1$  depends on both  $g$  and  $\tilde{\mu}$ . This task is done by expanding all variables systematically in powers of  $\lambda$  and writing down a set of successive equations to each order. The solution thus found is continuously connected to the free Fermi gas, and satisfies the Luttinger-Ward volume theorem at  $T = 0$ . The latter is an essential part of claiming that the resulting theory is a variety of Fermi liquid, being notoriously difficult to satisfy in uncontrolled approximations such as the truncations of Green's function equations. On setting the time-dependent potential to zero we get the frequency-dependent Green's function as

$$G(k, i\omega_j) = g(k, i\omega_j) \times \tilde{\mu}(k, i\omega_j) \\ = \frac{1 - \lambda\frac{n}{2} + \lambda\Psi(\vec{k}, i\omega_j)}{g_0^{(-1)}(\vec{k}, i\omega_j) - \lambda\Phi(\vec{k}, i\omega_j)}, \quad (7)$$

where the two self-energies  $\Psi, \Phi$  determine  $G$ . The ECFL formalism has a systematic expansion of these equations in powers of  $\lambda$ , starting with the free Fermi gas as the lowest term and finally setting  $\lambda = 1$ . An expansion in  $\lambda$  thus provides a controlled framework for explicit calculations [1,15]. The current version of the theory [1–3,15] is valid to  $O(\lambda^2)$  and has been benchmarked against other standard techniques for strong coupling in limiting cases of infinite dimensionality [i.e., dynamical mean field theory (DMFT)] and the single-impurity limit [15]. Higher-order terms in  $\lambda$  are expected to impact the results outside the regime considered here, namely  $0.13 \lesssim \delta \lesssim 0.2$ . It has been recently applied to several objects of experimental interest such as angle-resolved photoemission (ARPES), Raman scattering, optical conductivity, the Hall constant, and recently the resistivity [2,3,16].

One of the main effects of strong correlations is to reduce significantly the quasiparticle weight  $Z$  from its Fermi gas value of unity. It is worth commenting that the exact DMFT studies of the Hubbard model in  $d = \infty$  using a mapping to a self-consistent Anderson impurity model yield a very small  $Z$  for  $U > 2.918D$  ( $2D$  is the bandwidth) as one approaches the insulating limit  $n \rightarrow 1$ . This is seen, e.g., in Fig. 1(a) of [21], where  $Z$  is plotted versus  $\delta = 1 - n$  for various  $U$ . One sees that  $Z$  decreases upon with increasing  $U$ , taking a nonzero value in the  $U = \infty$  limit. In this limit its density dependence is close to the empirical formula  $Z \sim \delta^{1.39}$ . In the case of the 2-d  $t$ - $t'$ - $J$  model the ECFL results [2] have

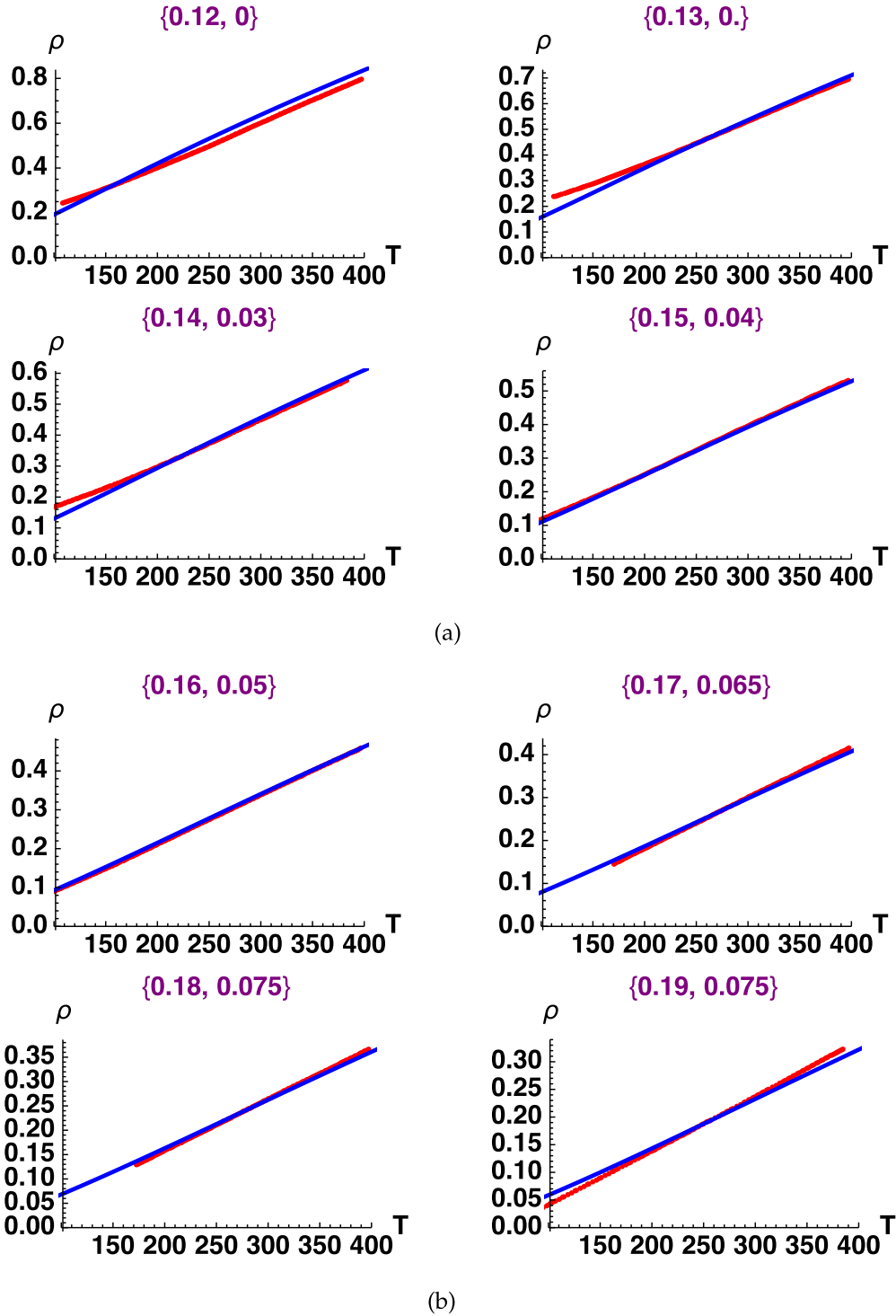


FIG. 1. (a) LSCO: Slightly underdoped to optimally doped. (b) LSCO: Near-optimal doping. The resistivity  $\rho$  is in units of  $\text{m}\Omega\text{ cm}$  and  $T$  is in kelvins. Dotted (red) line is data extracted from Fig. 2(b) of Ando and co-workers [22], and solid (blue) curve is the theoretical curve with  $t'/t = -0.2$ . Panels (a) and (b) focus on densities in the slightly underdoped and near-optimal doping ranges. The displayed pair of numbers  $\{\delta, \rho_{\text{imp}}\}$  indicates the hole density and estimated impurity resistivity. The parameter  $t = 0.9$  eV was fixed using  $\Gamma(T^\Phi)$ , the slope of the resistivity [see Eq. (9)] at  $\delta = 0.15$ ,  $T^\Phi = 250$  K in panel (a). The resistivities at every other density in other panels and in the three panels of Fig. 2 are then predicted by the theory.

a similar character. The reduction of  $Z$  from unity occurs as we approach the insulating limit  $n \rightarrow 1$ . Additionally, it is very sensitive to the sign and magnitude of  $t'/t$  [23]. The dependence of  $Z$  on  $n$  and  $t'/t$  is most clearly seen in

Fig. 1 of [2]. Qualitatively we find that  $Z$  decreases when  $t'/t$  is negative and growing in magnitude, whereas a positive  $t'/t$  enhances its value. Within the theory, reduction of the magnitude of  $Z$ , i.e., the loss of weight of the quasiparticles, is

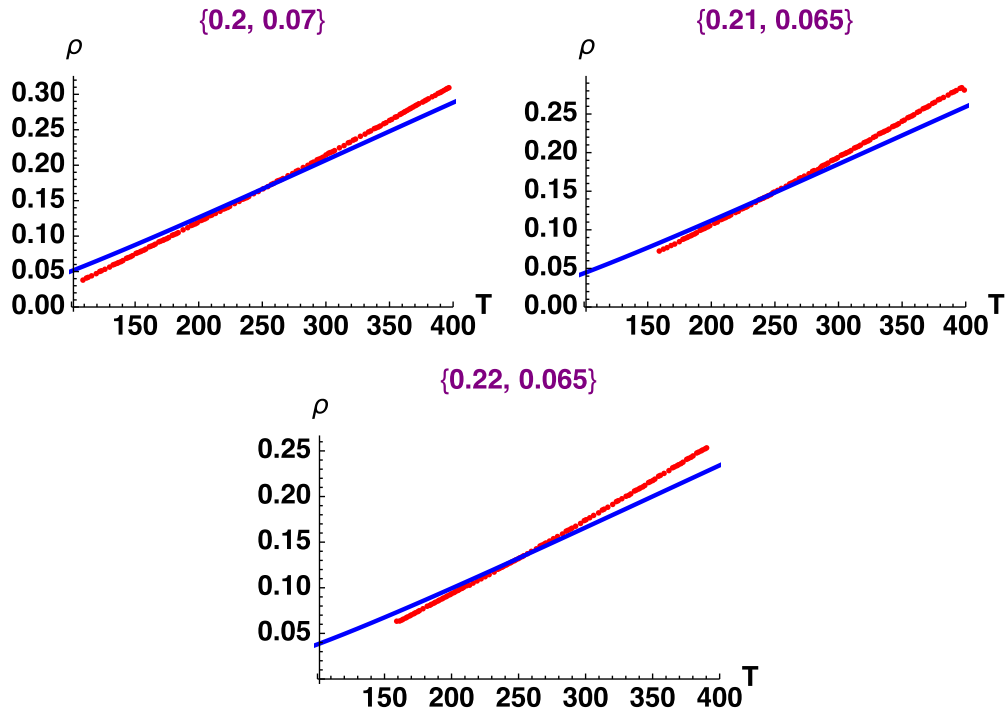


FIG. 2. The resistivity  $\rho$  is in units of  $\text{m}\Omega \text{ cm}$  and  $T$  is in kelvins. Dotted (red) line is data extracted from Fig. 2(b) of Ando and co-workers [22] for the slightly overdoped cases of LSCO, and solid (blue) curve is the theoretical curve with  $t'/t = -0.2$  and  $t = 0.9 \text{ eV}$ .

compensated exactly by the growth of the background pieces of the spectral function, as seen in Figs. 1–2 of [3]. We note that experiments on cuprates strongly indicate the growth of background weight, and indeed the ECFL theoretical results closely match experiments in regard to the shapes of spectral functions [16].

The resistivity calculations in Refs. [2,3] were performed for a typical set of model parameters chosen for illustrative purposes. In these works we noted that the resulting resistivities are broadly comparable to experiments in their magnitude and on the scale of temperature variation. In the present paper we push this observation to a more explicit and quantitative level, by comparing the ECFL results of [2,3] with experiments on a few representative high- $T_c$  materials with both hole and electron doping. Although broken symmetries of various types are possible within the methodology, we focus here on the properties of the paramagnetic normal state.

### III. PARAMETERS OF THE MODEL

The ECFL theory results used here [2,3] are valid for a quasi-two-dimensional correlated metal, with separation  $c_0$  between layers. The resistivity in the calculations [2,3] arises from intrinsic inelastic  $e$ - $e$  scattering with the umklapp processes, inherent in the tight-binding model, relaxing the momentum efficiently. The (smaller)  $a$  and  $b$  axis lattice constants cancel out in the formula for resistivity. The theory gives the planar resistivity in the form

$$\rho = R_{vK} \times c_0 \times \bar{\rho} \left( \frac{t'}{t}, \frac{J}{t}, \frac{k_B T}{t}, \delta \right), \quad (8)$$

where  $R_{vK} = \frac{h}{e^2} = 25813 \Omega$  is the von Klitzing resistance. The (dimensionless) theoretical resistivity  $\bar{\rho}$  is a function of

the four displayed dimensionless variables. Detailed formulas leading to this expression can be found in Eqs. (45) and (46) of [2] and Eqs. (12) and (13) of [3]. More precisely  $\delta$  is the concentration of holes measured from half filling, i.e.,  $\delta = 1 - n$  and  $n = \frac{N_e}{N_s}$ , where  $N_e$  ( $N_s$ ) is the number of electrons (copper sites). At  $\delta = 0$  ( $n = 1$ ) the model describes a Mott-Hubbard insulator. We discuss below the exchange parameter  $J/t$ , which plays a secondary role at the densities considered here. While three parameters  $c_0$ ,  $\delta$ ,  $T$  are obtained from experiments directly, ARPES constrains the parameter  $t'/t$  from the shape of the Fermi surface in most cases. Given these, the remaining single parameter  $t$  fixes the resistivity on an absolute scale. In addition the usually small and  $T$ -independent (extrinsic) impurity resistance, usually arising from scatterers located off the 2-d planes, must be estimated separately.

In addition to  $c_0$ , the basic parameters of the model are the nearest-neighbor hopping  $t$ , the second-neighbor hopping  $t'$ , and a superexchange energy  $J$  within a tight-binding description of the copper  $d$ -like bands. The parameter  $t'$  plays an important role in distinguishing between hole-doped superconductors ( $t' < 0$ ) with a positive Hall constant and the electron-doped superconductors ( $t' > 0$ ) with a negative Hall constant. The shape of the Fermi surface is sensitive to the ratio of the bare hopping parameters  $t'/t$ , if one assumes that interactions do not change its shape very much; this is largely borne out in ECFL theory. For this reason ARPES can most often provide us with a good estimate for this parameter  $t'/t$ , although  $t$  itself is not fixed by knowing the shape of the Fermi surface. We fix  $J$  at a typical value  $0.17t$ . At the densities we study here we find that the magnitude of  $J$  has a very limited influence on the calculated resistivity, as seen, e.g., in Fig. 24 of [3]. For the single-layer cuprate systems, one has two Cu-O

layer per unit cell and therefore the separation  $c_0$  equals half the  $c$ -axis lattice constant  $c_L$  [24,25]. The applicability of the theoretical calculations to systems with a higher number of layers per unit cell, such as Bi-2212 or  $\text{YBa}_2\text{Cu}_3\text{O}_{6-\delta}$ , is less direct. It requires making further assumptions relating  $c_0$  to the lattice constants. In order to avoid this we confine ourselves to single-layer systems.

The theoretical results tested here are found by ignoring a possible superconducting or magnetic state. We have produced a grid of theoretical calculations for  $t'/t = -0.4, -0.3, \dots, 0.3$  at several densities in the range  $0.12 \leq \delta \leq 0.22$  surrounding the interesting regime of optimal doping  $\delta \sim 0.15$ . Since the theory is smooth in most theoretical parameters we can interpolate in it, when necessary. Calculations are carried out in a wide range of  $T$  with a lower end  $T \sim 100$  K with a system size of  $62 \times 62$ . Lower  $T$  calculations require bigger system sizes which are computationally expensive and alternate methods are possible for estimating the resistivity. For example at lower  $T \lesssim 50$  K the resistivity can be extrapolated to a quadratic in  $T$  quite accurately using  $\rho = \alpha T^2 / (1 + T/T_0)$  with suitable constants  $\alpha, T_0$ . This form is consistent with the  $T \rightarrow 0$  Fermi liquid character of the theory below the (already low)  $T_0$

#### IV. THE CHOICE OF SYSTEMS

The lattice structure of the cuprates allows for a systematic change in carrier concentration by chemical substitution of elements situated away from the copper oxide planes, without severely impacting the impurity resistance. The role of block layers or charge reservoirs in hosting the donors away from the copper oxide planes plays an important role in achieving this property of the cuprates [24,25]. This feature also provides a useful handle in our analysis; we can access data on families of cuprates that contain a reasonably large range of electron densities. Since the basic parameters of the theoretical model can be assumed unchanged with doping [26], such a family provides a systematic proving ground for theory. Thus the experimental data used for testing the theory are narrowed down to the available systematic sets of resistivity data on single-layer cuprates with varying densities.

In Table I we list the single-layer cuprate compounds where data sets with several densities are available. The hole-doped LSCO and BSLCO materials are well studied by many authors, and the data set from Ref. [22] used here reports a very extensive set of densities for each family. This provides us with 11 densities for LSCO in the range  $0.12 \leq \delta \leq 0.22$  and 7 densities for BSLCO in the range  $0.12 \leq \delta \leq 0.18$  which are essentially within the range treatable by theory. We include recent thin-film data on the electron-doped LCCO from Ref. [27]. Here 4 densities are available in the theoretical range and the very regular  $\rho \sim +T^2$  type behavior of the data allows for easily eliminating the impurity contribution. For a more balanced representation of the electron-doped materials, we included data on NCCO from Ref. [28]. The NCCO family contains only two densities in the theoretically accessible range, of which one is impacted by 2-d localization effects. It is therefore not as constraining as the other families. The choice of the above four families of single-layer cuprates with

TABLE I. The single-layer cuprates analyzed in this work. For the first three materials the values of  $t'/t$  are obtained from ARPES experiments where the Fermi surface shape is fitted to a tight-binding model. For LCCO the ARPES data on the Fermi surface do not exist. The quoted  $t'/t$  is chosen to be the same as NCCO. The resistivity data for LCCO are from thin films while the other data are from single crystals. Here  $c_L$  is the  $c$ -axis lattice constant. In all the above cases the unit cell contains two copper oxide layers, and hence their separation  $c_0$  entering Eq. (8) is half the lattice constant  $\frac{1}{2}c_L$ . The last column lists the values of  $t$  determined in this work. The single adjustable parameter, the hopping  $t$ , is found using the slope of the experimental resistivity at 200 K at a single density  $\delta = 0.15$  as in Eq. (9). Band structure estimates of the  $t'/t$  ratio [29,30] are quite close to the ones used here, but the estimates of  $t$  differ somewhat. It must be kept in mind that the quoted parameter  $t$  is the bare one, i.e., prior to many-body renormalization.

Single-Layer High- $T_c$ Compounds			
Material	$c_L$ (Å)	$t'/t$	$t$ (eV)
$\text{La}_{2-x}\text{Sr}_x\text{CuO}_4$ (LSCO)	13.25 [22,31]	-0.2 [32,33]	0.9
$\text{Bi}_2\text{Sr}_{2-x}\text{La}_x\text{CuO}_6$ (BSLCO)	24.3 [22]	-0.25 [33]	1.35
$\text{Nd}_{2-x}\text{Ce}_x\text{CuO}_4$ (NCCO)	12.01 [24,34]	+0.2 [35]	0.9
$\text{La}_{2-x}\text{Ce}_x\text{CuO}_4$ (LCCO)	12.45 [36]	+0.2	0.76

$\gtrsim 20$  sample densities seemed sufficiently representative for our task.

In addition to the above set of materials there are a few others belonging to the single-layer class with data provided for several densities. Among these we have excluded from our analysis the mercury compound Hg1201 ( $\text{HgBa}_2\text{CuO}_{4+\delta}$ ) [37] and the thallium compound Tl2201 ( $\text{Tl}_2\text{Ba}_2\text{CuO}_{6+\delta}$ ) [38,39]. In the literature for these compounds, the value of  $T_c$  for different samples is quoted and one needs to extract the electron density from other measurements, e.g., the Hall constant. This was hard for the authors to achieve, with a required accuracy in density  $\Delta\delta \sim 0.1$  necessary for the present analysis.

In Table I we quote the  $c$ -axis lattice constant  $c_L$  taken from x-ray diffraction data. The ratio  $t'/t$  is taken from angle-resolved photoemission (ARPES) experiments on the shape of the Fermi surface, fitted to a tight-binding band. In some cases the experimental fits include a small further neighbor hopping as well; we neglect it here since the corrections only fine-tune the shapes of the Fermi surface while preserving their basic topology. Theoretical estimates from band structure [29,30] are roughly consistent with the above experimentally guided choices of  $t'/t$ .

#### V. PROTOCOL FOR FIXING $t$ AND ESTIMATING THE IMPURITY RESISTIVITY

We determine the magnitude of  $t$  for each material by collating a data set consisting of experimental  $\rho_{\text{exp}}(T, \delta)$  points at various densities  $\delta = \delta_1, \delta_2, \dots$ . From this set we extract the slope of the resistivity

$$\Gamma(T^\Phi) = \left( \frac{d\rho_{\text{exp}}(T, \delta = 0.15)}{dT} \right)_{T=T^\Phi}. \quad (9)$$

Equating  $\Gamma(T^\Phi)$  to the corresponding theoretical slope at  $T^\Phi$  determines the single parameter  $t$ . The density is chosen as  $\delta = 0.15$  since it is in a regime where the calculation is quite reliable.  $T^\Phi$  is chosen as the midpoint of the temperature range of the data set, so that  $T^\Phi = 250$  K for LSCO and  $T^\Phi = 200$  K for BSLCO and LCCO in the following analysis.

We next need to estimate the  $T$ -independent impurity contribution to the resistivity at each density  $\rho_{\text{imp}}(\delta)$  for LSCO and BSLCO [40]. For LCCO the impurity contribution  $\rho_{\text{imp}}$  has been eliminated by the authors of [27]; thus this task is already done. For the others we shift down the experimental resistivity  $\rho_{\text{exp}}(T^\Phi, \delta)$  to match the theoretical resistivity; the magnitude of the shift gives us the estimated  $\rho_{\text{imp}}(\delta)$  at each density. We are thus using the relation  $\rho_{\text{exp}}(T^\Phi, \delta) - \rho_{\text{imp}}(\delta) = \rho_{\text{th}}(T^\Phi, \delta)$ , where  $\rho_{\text{th}}$  is from Eq. (8). The impurity contribution is displayed in all figures and is a small fraction of the total resistivity in all cases.

In summary fixing the magnitude of  $t$  for a data set requires a comparison with experiments at a *single density* ( $\delta = 0.15$ ) and a *single temperature* ( $T = T^\Phi$ ). The impurity contribution is estimated at each density at the same temperature  $T = T^\Phi$ . Checking these against data constitutes the essence of the test carried out here. The final two columns in Table I report the fitted value of the single undetermined parameter  $t$ . The bare bandwidth is estimated as  $W \sim 8t$ . Slightly different choices of the density and  $T^\Phi$  lead to comparable results for  $t$ .

Before looking at the results, we make a few comments about the analysis. (a) The requirement that the fitted values of  $t$  and  $t'/t$  remain unchanged for different densities  $\delta$  gives added significance to the fits. It is clearly an important and nontrivial requirement from any theory as well. In this sense matching the experimental resistivity at a single density of any particular compound is less significant than doing so at a sequence of different densities. (b) The impurity shifts reported in each curve are seen to be on a typically expected scale  $\sim 50\text{--}150 \mu\Omega \text{ cm}$ . The data on LCCO [27] are available with the impurity contribution already removed by the authors. (c) At low electron densities the effects of (2-d) electron localization are visible in some data sets. In these cases the impurity contribution leads to an upturn at low  $T$ . This upturn has been discussed extensively in the literature [22,28] and also manipulated with magnetic fields [41]. Since the ECFL theory excludes any strong-disorder effects, we do not expect to capture these in the fits.

For LCCO the digital data were provided by the authors of [27]. For the other data sets studied here the published resistivity data were digitized using the commercial software program DigitizeIt [42]. We found that the program works quite well provided the experimental curves do not overlap or cross. This feature limited our data extraction to some extent, as the reader might notice from the low-temperature truncation in the experimental data in the figures presented below.

We next describe the comparison for different systems.

## VI. LSCO

In Figs. 1(a) and 1(b) and Fig. 2 the extensive data set from Fig. 2(b) of [22] is compared with theoretical predic-

tions. The parameters in Table I are used here. The band parameter  $t = 0.9$  eV is found from the slope of the resistivity  $\delta = 0.15$ ,  $T^\Phi = 250$  K. All other densities are then predicted by theory on an absolute scale. While some deviations at low density  $\delta = 0.12$  and also at high density  $\delta \gtrsim 0.2$  are visible, the overall agreement seems fair. For the same parameters Fig. 6(a) shows the theoretical resistivity over an enlarged temperature window. Here subtle changes of curvature are visible at high and low  $T$ .

## VII. BSLCO and Bi-2201

In Fig. 3 the data for the BSLCO family of compounds  $\text{Bi}_2\text{Sr}_{2-x}\text{La}_x\text{CuO}_6$  from Ando [22] is compared with theory. The band parameter  $t = 1.35$  eV is found from the slope of the resistivity at  $\delta = 0.15$ ,  $T^\Phi = 200$  K. All other densities are then predicted by theory. For these parameters Fig. 6(b) shows the theoretical resistivity over an enlarged temperature window. The larger value of  $t$  in BSLCO relative to that in LSCO can be understood from comparing Figs. 6(a) and 6(b). The almost doubled value of  $c_0$  increases by a similar factor the resistance of BSLCO over that of LSCO, provided one is at the same scaled temperature  $T/t$ . A larger  $t$  spreads this increase over a larger  $T$  window.

## VIII. NCCO AND LCCO

The NCCO family of materials with composition  $\text{Nd}_{2-x}\text{Ce}_x\text{CuO}_4$  and the closely related LCCO family  $\text{La}_{2-x}\text{Ce}_x\text{CuO}_4$  are of considerable interest as counterpoints to the other two families studied above. Both have the opposite sign of the Hall constant from the hole-doped cases and display a pronounced  $T^2$ -type resistivity.

In a single band model description, such as the  $t$ - $t'$ - $J$  model used here, these materials can also be treated as having a filling less than half. The filling of these materials in the original electron picture is greater than half. Starting with a Hubbard model one can perform a particle-hole transformation of both spin species to map the model to less than half filling. For  $U$  large enough the  $t$ - $J$  model is once again introduced in the place of the Hubbard model. This process generates some  $U$ -dependent constant terms that are absorbed into the chemical potential. It also flips the sign of all hopping matrix elements. While the nearest-neighbor hopping  $t$  can be flipped back to the standard (positive) sign using a simple unitary transformation (exploiting the square lattice geometry), the second-neighbor hopping  $t'$  is now positive and the Fermi surface is electron-like.

On the materials side, the available data on NCCO [28] [see Fig. 9(b) therein] is relatively sparse in the metallic range containing only two samples. One of these is afflicted with strong-disorder effects at low  $T$ . In Fig. 4 we compare the data from Onose and co-workers [28] with theory. While the density  $\delta = 0.15$  is perfectly matched with theory, the lower density  $\delta = 0.125$  curve shows a distinct upturn at low  $T$ , as discussed in [28]. A systematic treatment of strong-disorder effects in the ECFL theory is currently missing.

The data on LCCO [27] give us four densities within the range covered by theory. In the absence of ARPES data we choose  $t'/t = 0.2$ , i.e., the same value as in NCCO. We have

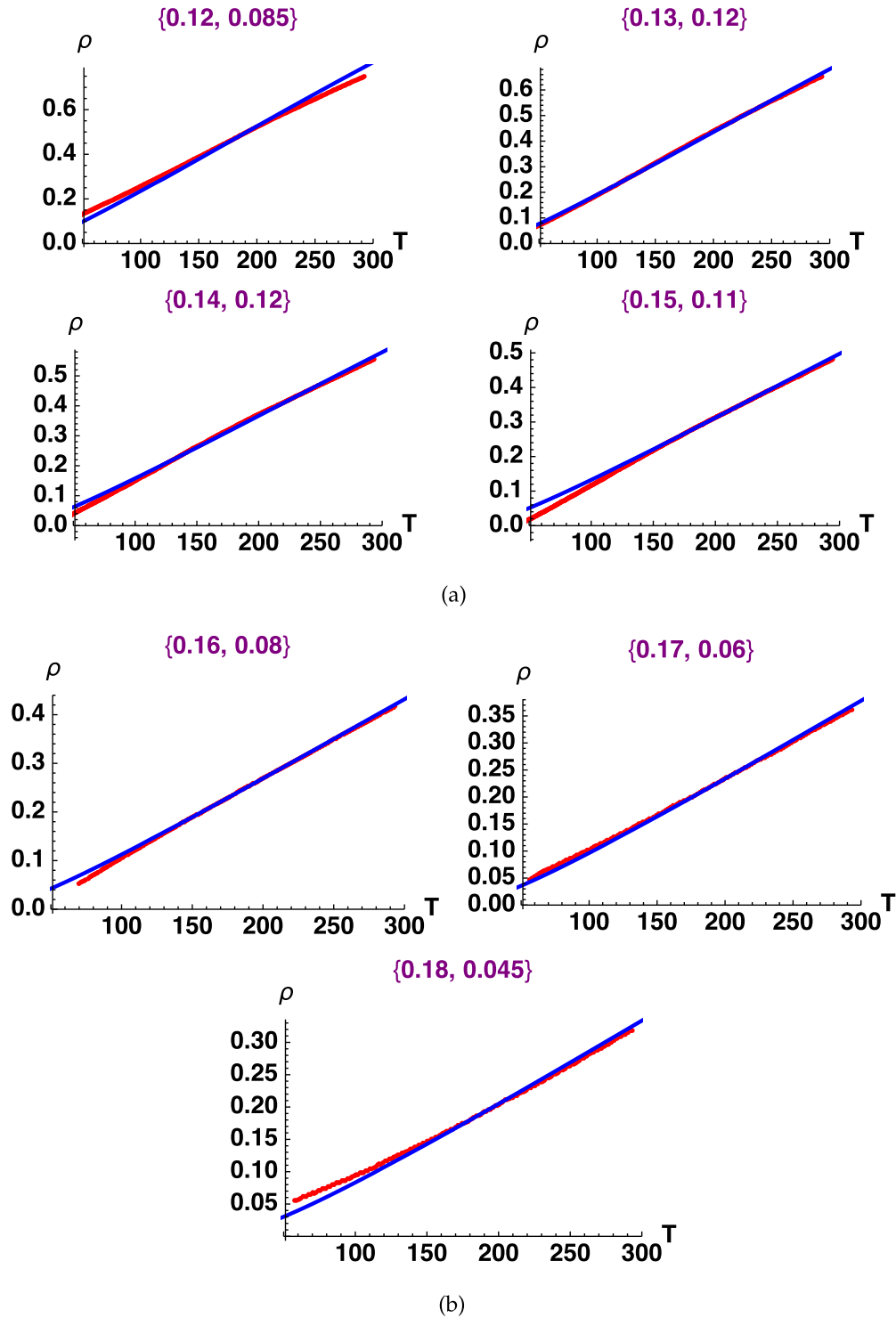


FIG. 3. (a) BSLCO: Slightly underdoped. (b) BSLCO: Near-optimal doping. The resistivity  $\rho$  is in units of  $\text{m}\Omega \text{ cm}$  and  $T$  is in kelvins. Dotted (red) line is data extracted from Fig. 1(a) of Ando and co-workers [22], and solid (blue) curve is the theoretical curve with  $t'/t = -0.25$ . Panels (a) and (b) focus on densities in the slightly underdoped and near-optimal doping ranges. The displayed pair of numbers  $\{\delta, \rho_{\text{imp}}\}$  indicates the hole density and estimated impurity resistivity. The parameter  $t = 1.35 \text{ eV}$  was fixed using  $\Gamma(T^\Phi)$ , the slope of the resistivity [see Eq. (9)] at  $\delta = 0.15$ ,  $T^\Phi = 200 \text{ K}$  in panel (a). The resistivity at every density in the other panels is then predicted by theory.

verified that nearby values to  $t'/t$  lead to a similar quality of fits after adjusting the parameter  $t$ , and hence this choice not final. The authors conveniently present the resistivity in Fig. 2(b) of [27] requiring no further impurity corrections. In

Fig. 5 we compare theory and experiment, and in Fig. 6(c) we present the theoretical resistivity on an extended  $T$  scale at several densities. The discrepancy in LCCO between theory and experiment at  $\delta = 0.17$  at  $T = 200$  is  $\sim 0.01$ , and is quite

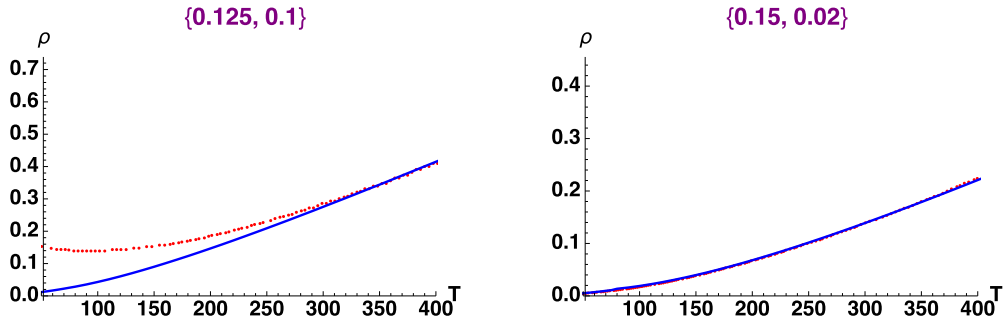


FIG. 4. The resistivity  $\rho$  is in units of  $\text{m}\Omega \text{ cm}$  and  $T$  is in kelvins. Dotted (red) line is data extracted from Fig. 9(b) of Onose and co-workers [28], and solid (blue) curve is the theoretical curve with  $t'/t = +0.2$ . The parameter  $t = 0.9 \text{ eV}$  was fixed using the slope of the  $\delta = 0.15$  data at 200 K. The data set contains only these two densities within the range accessible to theory. The upturn in the lower density curve and the larger magnitude of impurity resistivity are due to strong disorder effects, as already noted in [27]. The sign of  $t'/t$  is reversed between this figure and Fig. 1 for LSCO, while other parameters  $c_0, t$  are essentially unchanged. Both the experimental and theoretical resistance display a resistance with a positive upward curvature (i.e.,  $\rho \sim +T^2$ ).

visible. However we should keep in mind that at corresponding densities the absolute scale of the resistivity for LCCO is considerably smaller than that for LSCO and BSLCO. This can be seen in Figs. 2 and 3. As a consequence a similar scale of absolute error leads to a much larger relative error.

### IX. DISCUSSION

We have presented a comparison of theoretical resistivity with extensive data on three families of cuprate superconductors. It is also feasible to fit data on noncuprate strongly correlated systems such as  $\text{Sr}_2\text{RuO}_4$  from [43], where data over a large range  $T \leq 1000$  are available. However data are

available at only one composition in this case, and the value of  $t'/t$  is hard to find from experiments. Since a single density within a family does not test the theory stringently, we omit the comparison here.

Overall we have shown that the ECFL theory gives a reasonable account of data in the three families discussed above. A small number of parameters taken from experimental data fix the model completely. It is encouraging that the resulting resistivity affords a reasonable fit to a collection of resistivity data at various densities, both in terms of the  $T$  dependence and its magnitude. It is also encouraging that upon using different model parameters, the same calculation

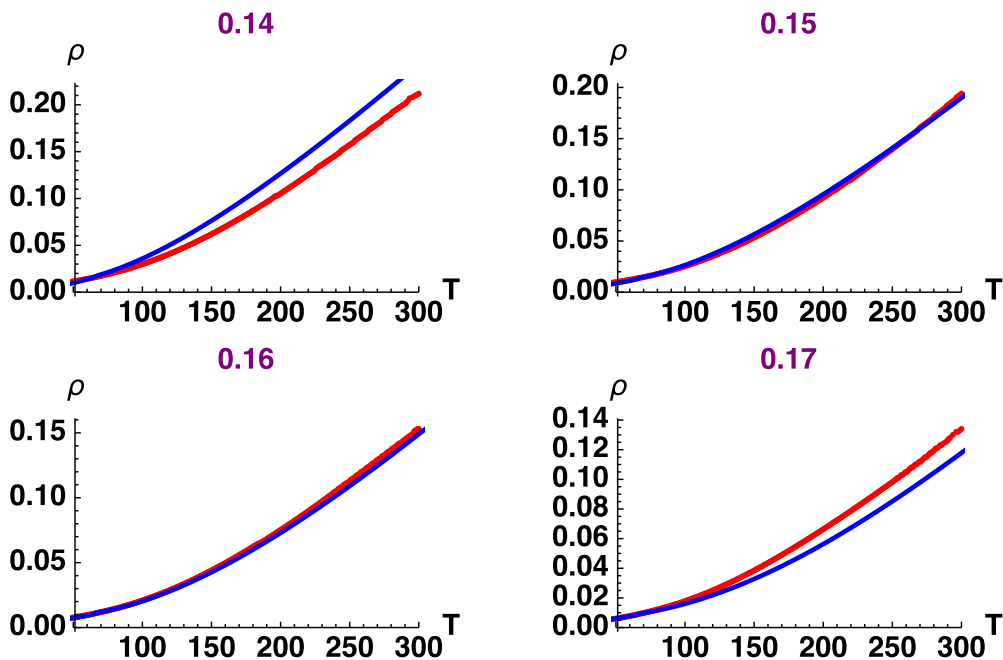


FIG. 5. The resistivity  $\rho$  is in units of  $\text{m}\Omega \text{ cm}$  and  $T$  is in kelvins. Data are from Fig. 2(b) of Sarkar and co-workers [27] as the dotted red line. The impurity contribution in this data set has been removed by the authors in [27]. The theoretical curve is in solid blue, with  $t'/t = +0.2$ . The hole density is marked at the top in each plot. The parameter  $t = 0.76 \text{ eV}$  was fixed using  $\Gamma(T^\Phi)$  [see Eq. (9)], the slope of the resistivity at  $\delta = 0.15, T^\Phi = 200 \text{ K}$ . The sign of  $t'/t > 0$  is common to NCCO and reversed from that in LSCO and BSLCO. Both experiments and theory find a resistance with a positive curvature (i.e.,  $\rho \sim +T^2$ ), as in NCCO. This is in striking contrast to LSCO and BSLCO as seen in Figs. 1, 2, and 3.



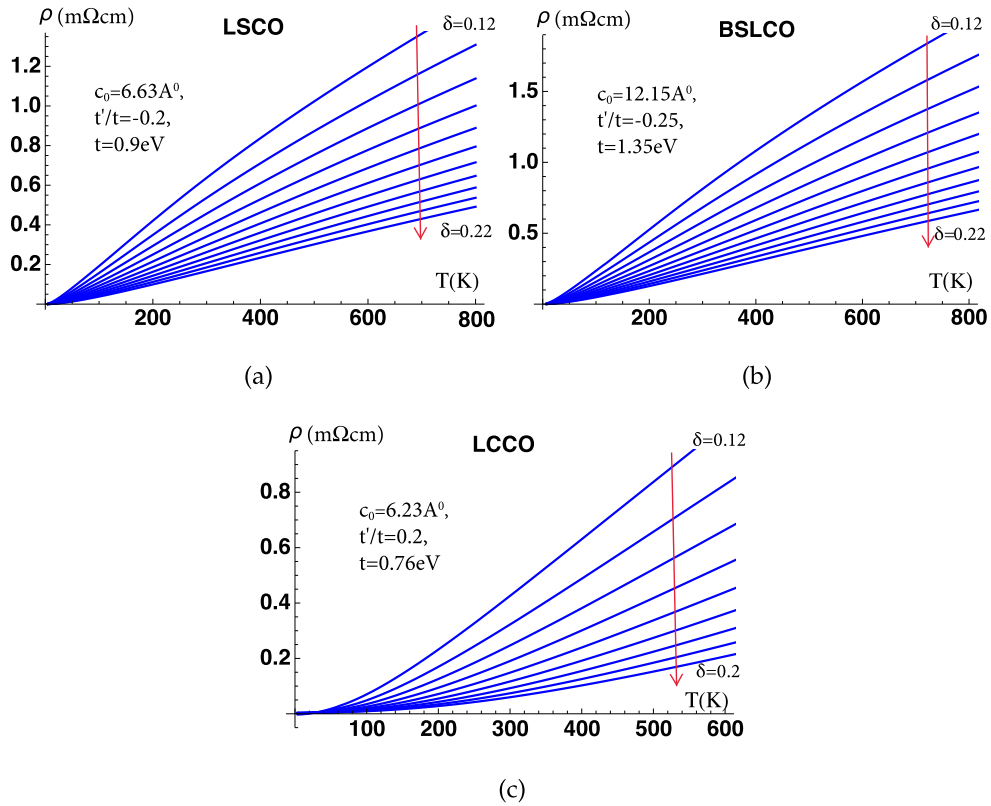


FIG. 6. (a) LSCO:  $\delta = 0.12 \rightarrow 0.22$  (increasing  $\downarrow$ ). (b) BSLCO:  $\delta = 0.12 \rightarrow 0.22$  (increasing  $\downarrow$ ). (c) LCCO:  $\delta = 0.12 \rightarrow 0.2$  (increasing  $\downarrow$ ). Theoretical resistivity curves for LSCO [panel (a)], BSLCO [panel (b)], and LCCO [panel (c)] over an extended temperature range. The hole densities increase downward at intervals  $\Delta\delta = 0.01$ . In going from LSCO with BSLCO the separation between the layers, i.e.,  $c_0$ , is almost doubled while  $t'/t$  changes only slightly. The resistivity at a comparable  $(\delta, T)$  here, and also in the data, changes by a smaller factor than  $c_0$ . In order to reconcile with this feature of the data, the deduced hopping parameter  $t$  is greater by  $\sim 50\%$  for BSLCO relative to LSCO. The distinct almost pure  $T^2$  behavior of the resistivity of LCCO relative to the other two systems is striking. Additionally it is noteworthy that the magnitude of the intrinsic resistivity of the electron-doped LCCO is considerably smaller than that of the hole-doped LSCO. Since these have roughly the same  $c_0$ ,  $t$ ,  $|t'/t|$  values, the difference is attributable to the different sign of  $t'/t$ .

fits the resistivity of both hole-doped and electron-doped materials.

In Fig. 6 we display the theoretical resistivities on a larger  $T$  scale and for more densities, using parameters of the three families separately. We found that the data are fitted almost equally well by making nearby choices of the pair  $t'/t$  and  $t$ . The differences between different choices do exist and show up but only at higher  $T$ , especially in the location of subtle kinks of the sort seen in Fig. 6.

## X. CONCLUSIONS

From the above exercise it appears that the extremely correlated Fermi liquid theory has the necessary ingredients to explain the variety of data seen in the above materials. Other materials, some of them with a higher number of layers, do display further subtle features which are missing in the theory. However these features are also missing in the displayed data from the above materials. We have thus made a fair beginning with the above “standard” cuprate materials, but further challenges from more complex behavior are to be expected.

A few comments on the results and their implications are appropriate. Let us first discuss the hole-doped materials. Here the quasilinear resistivity seen near  $\delta \sim 0.15$  is remarkable, as noted by many authors. We should also pay attention to the underlying suppression of scale. By this we refer to the fact that the temperature scale of resistivity variation is as low as  $\sim 100$ - $300$  K, starting from a bare bandwidth of almost  $10$  eV. The three orders of magnitude reduction in scale is nontrivial, reminiscent of the emergence of the low-energy Kondo scale in magnetic impurity systems. Starting from wide energy bands with a width of  $\sim 10$  eV, the ECFL theory systematically generates low energy and temperature scales, a few orders of magnitude smaller than the bare ones [1,15,16]. The low energy scales depend sensitively on the density and a few other parameters, especially the sign and magnitude of  $t'/t$ .

A major part of this scale suppression is due to the small quasiparticle weight  $Z \lesssim 0.1$  at relevant densities that arise in the theory [1–3]. More physically we can attribute this suppression to the profound role of Gutzwiller projection on the electron propagators near the Mott-Hubbard half-filled limit. It is captured to a good extent by the ECFL theory,

and is visible in the detailed structure of the electron spectral functions [1–3].

For the electron-doped materials, it is interesting that the theoretical resistivity matches experiments essentially as well as for the hole-doped materials. The two classes of materials have the opposite sign of the parameter  $t'/t$ , which is disconnected from the extent of correlations. This finding has a bearing on the frequently debated topic of the Fermi liquid nature of electron-doped cuprates. The ECFL theory says that both hole-doped and electron-doped systems are (extremely correlated) Fermi liquids at the lowest temperature. Additionally the theory quantifies the range of  $T$  where a Fermi liquid type behavior  $\rho \sim T^2$  holds good. Going further it also identifies regimes succeeding the Fermi liquid [1–3,15,44,45] upon warming.

In order to better understand the origin of the difference between hole and electron doping within the theory, the following observation may be helpful. It is known that the sign and magnitude of the parameter  $t'/t$  directly influences the magnitude of the already small quasiparticle weight  $Z$  (see Fig. 1 of [2]) [23]. A positive  $t'/t$  leads to a small  $Z$ , while a negative  $t'/t$  leads to an even smaller but nonvanishing  $Z$ . For the electron-doped case this distinction ultimately results in an enhanced thermal range displaying a positive curvature

of the  $\rho$ - $T$  plots. The effect on resistivity of the sign of  $t'/t$  can be seen explicitly by comparing the theoretical resistivity curves for the hole-doped cases Figs. 6(a) and 6(b) with the electron-doped case in Fig. 6(c).

As a cross-check on the theory, it would be interesting to compare other physical variables with data for the systems considered here, using the deduced parameters. Finally we should note that future technical developments in the implementation of the ECFL theory are likely to refine some of the theoretical results presented here.

## ACKNOWLEDGMENTS

We are grateful to Professor A. J. Leggett for stimulating discussions and for valuable comments on the manuscript. We thank Prof. R. L. Greene and Dr. T. Sarkar for providing the digitized resistivity data of [27]. We also thank Prof. Y. Ando, Prof. M. Greven, and Prof. A. Ramirez for useful comments. The work at UCSC was supported by the US Department of Energy (DOE), Office of Science, Basic Energy Sciences (BES), under Award No. DE-FG02-06ER46319. The computation was done on the Comet in XSEDE [46] (TG-DMR170044) supported by National Science Foundation Grant No. ACI-1053575.

- 
- [1] B. S. Shastry, *Phys. Rev. Lett.* **107**, 056403 (2011).  
 [2] B. S. Shastry and P. Mai, *New J. Phys.* **20**, 013027 (2018).  
 [3] P. Mai and B. S. Shastry, *Phys. Rev. B* **98**, 205106 (2018).  
 [4] P. W. Anderson, *Phys. Rev. B* **78**, 174505 (2008); P. W. Anderson and Z. Zou, *Phys. Rev. Lett.* **60**, 132 (1988).  
 [5] C. M. Varma, P. B. Littlewood, S. Schmitt-Rink, E. Abrahams, and A. E. Ruckenstein, *Phys. Rev. Lett.* **63**, 1996 (1989).  
 [6] T. Moriya, Y. Takahashi, and K. Ueda, *J. Phys. Soc. Jpn.* **59**, 2905 (1990).  
 [7] P. Monthoux, A. V. Balatsky, and D. Pines, *Phys. Rev. Lett.* **67**, 3448 (1991).  
 [8] A. S. Alexandrov, V. V. Kabanov, and N. F. Mott, *Phys. Rev. Lett.* **77**, 4796 (1996).  
 [9] R. Zeyher and M. L. Kulić, *Phys. Rev. B* **53**, 2850 (1996); **54**, 8985 (1996); A. Greco and R. Zeyher, *Europhys. Lett.* **35**, 115 (1996).  
 [10] N. M. Plakida and V. S. Oduenko, *Phys. Rev. B* **59**, 11949 (1999).  
 [11] G. Kastinakis, *Phys. C (Amsterdam)* **340**, 119 (2000); *Phys. Rev. B* **71**, 014520 (2005).  
 [12] P. Phillips, *Philos. Trans. R. Soc. A* **369**, 1574 (2011).  
 [13] A. A. Patel and S. Sachdev, *Phys. Rev. Lett.* **123**, 066601 (2019).  
 [14] I. J. Robinson, P. D. Johnson, T. M. Rice, and A. M. Tsvelik, *Rep. Prog. Phys.* **82**, 126501 (2019).  
 [15] B. S. Shastry and E. Perepelitsky, *Phys. Rev. B* **94**, 045138 (2016); P. Mai, S. R. White, and B. S. Shastry, *ibid.* **98**, 035108 (2018).  
 [16] P. Mai and B. S. Shastry, *Phys. Rev. B* **98**, 115101 (2018); K. Matsuyama, E. Perepelitsky, and B. S. Shastry, *ibid.* **95**, 165435 (2017); G.-H. Gweon, B. S. Shastry, and G. D. Gu, *Phys. Rev. Lett.* **107**, 056404 (2011).  
 [17] The  $J$  part of the  $t$ - $J$  model for the insulator was introduced by P. W. Anderson, in *Solid State Physics*, edited by F. Seitz and D. Turnbull (Academic Press, Inc., New York, 1963), Vol. 14, p. 99; Using Kohn's general canonical transformation, A. B. Harris and R. Lange [*Phys. Rev.* **157**, 295 (1967)] derived the correct form of the kinetic energy in the lower Hubbard band [see Eq. (4.49b)]. The bare-bones version of the  $t$ - $J$  model used here, and in much of the literature, consists of this reduced kinetic energy and the superexchange term. We ignore the additional three-site correlated hopping terms arising from a canonical transform discussed by K. A. Chao, J. Spalek, and A. M. Oles [*J. Phys. C* **10**, L271 (1977)].  
 [18] P. W. Anderson, *Science* **235**, 1196 (1987); The glare of attention on the  $t$ - $J$  model appears to have begun with this paper.  
 [19] M. Ogata and H. Fukuyama, *Rep. Prog. Phys.* **71**, 036501 (2008) give a useful review of the  $t$ - $J$  model and some results using early techniques.  
 [20] B. S. Shastry, *Ann. Phys.* **343**, 164 (2014).  
 [21] R. Žitko, D. Hansen, E. Perepelitsky, J. Mravlje, A. Georges, and B. S. Shastry, *Phys. Rev. B* **88**, 235132 (2013); B. S. Shastry, E. Perepelitsky, and A. C. Hewson, *ibid.* **88**, 205108 (2013).  
 [22] Y. Ando, S. Komiya, K. Segawa, S. Ono, and Y. Kurita, *Phys. Rev. Lett.* **93**, 267001 (2004).  
 [23] The quasiparticle weight  $Z$  is given at various fillings and  $t'/t$  in Fig. 1 of [2]. The rapid plunge of the spectral function peaks in the Brillouin zone with warming are shown in Fig. 3 of [2]. Note that  $T$  is scaled by  $t$ , and the value of  $t$  in this figure is fixed at  $t = 0.45$  eV in [2]. Therefore  $T$  (and  $t$ ) must be rescaled for different materials as per the values discussed in Table I.  
 [24] Y. Tokura and T. Arima, *Jpn. J. Appl. Phys.* **29**, 2388 (1990).  
 [25] A. J. Leggett, *Quantum Liquids* (Oxford University Press, Oxford, 2006); see especially Sec. 7.2.

- [26] The lattice constant in many cuprates actually changes by a few percent with doping, as discussed by N. R. Khasanova and E. V. Antipov, *Phys. C (Amsterdam)* **246**, 241 (1995) and in [31,34]. While it is easy enough to accommodate this change in our calculation, it makes a relatively small difference and we neglect it here. Our comment on fixed parameters refers more strongly to the value of  $t'/t$  which can be taken as unchanged in a given family of compounds with varying densities.
- [27] T. Sarkar, R. L. Greene, and S. Das Sarma, *Phys. Rev. B* **98**, 224503 (2018).
- [28] Y. Onose, Y. Taguchi, K. Ishizaka, and Y. Tokura, *Phys. Rev. B* **69**, 024504 (2004) (see Fig. 10).
- [29] R. Markiewicz, *Phys. Rev. B* **72**, 054519 (2005).
- [30] E. Pavarini, I. Dasgupta, T. Saha-Dasgupta, O. Jepsen, and O. K. Andersen, *Phys. Rev. Lett.* **87**, 047003 (2001).
- [31] S. Kanbe, K. Kishio, K. Kitazawa, K. Fueki, H. Takagi, and S. Tanaka, *Chem. Lett.* **547** (1987).
- [32] T. Yoshida, T. Yoshida, X. J. Zhou, D. H. Lu, S. Komiya, Y. Ando, H. Eisaki, T. Kakeshita, S. Uchida, Z. Hussain, Z.-X. Shen, and A. Fujimori, *J. Phys.: Condens. Matter* **19**, 125209 (2007).
- [33] M. Hashimoto, T. Yoshida, H. Yagi, M. Takizawa, A. Fujimori, M. Kubota, K. Ono, K. Tanaka, D. H. Lu, Z.-X. Shen, S. Ono, and Y. Ando, *Phys. Rev. B* **77**, 094516 (2008).
- [34] P. K. Mang, S. Larochelle, A. Mehta, O. P. Vajk, A. S. Erickson, L. Lu, W. J. L. Buyers, A. F. Marshall, K. Prokes, and M. Greven, *Phys. Rev. B* **70**, 094507 (2004).
- [35] D. M. King, Z.-X. Shen, D. S. Dessau, B. O. Wells, W. E. Spicer, A. J. Arko, D. S. Marshall, J. DiCarlo, A. G. Loeser, C. H. Park, E. R. Ratner, J. L. Peng, Z. Y. Li, and R. L. Greene, *Phys. Rev. Lett.* **70**, 3159 (1993).
- [36] A. Sawa, M. Kawasaki, H. Takagi, and Y. Tokura, *Phys. Rev. B* **66**, 014531 (2002).
- [37] D. Pelc, M. J. Veit, C. J. Dorow, Y. Ge, N. Barišić, and M. Greven, [arXiv:1902.00529](https://arxiv.org/abs/1902.00529).
- [38] T. Manako, Y. Kubo, and Y. Shimakawa, *Phys. Rev. B* **46**, 11019 (1992).
- [39] J. Kokalj, N. E. Hussey, and R. H. McKenzie, *Phys. Rev. B* **86**, 045132 (2012).
- [40] Extrapolating the normal state resistivity to  $T \rightarrow 0$  is possible for some densities where the  $T$  dependence is purely linear (or purely quadratic) over most of the range. In such a case extrapolation gives the same result as our procedure. For general cases with a more complex  $T$  dependence, extrapolation requires an indeterminate fitting function. Our procedure then corresponds to choosing the fitting function as in the panels of Fig. 6 (all vanishing as  $T \rightarrow 0$ ) plus an impurity contribution.
- [41] G. S. Boebinger, Y. Ando, A. Passner, T. Kimura, M. Okuya, J. Shimoyama, K. Kishio, K. Tamasaku, N. Ichikawa, and S. Uchida, *Phys. Rev. Lett.* **77**, 5417 (1996).
- [42] I. Bormann, DigitizeIt (version 2.0), <http://www.digitizeit.de>.
- [43] H. Berger, L. Forro, and D. Pavuna, *Eur. Phys. Lett.* **41**, 531 (1998).
- [44] W. Ding, R. Žitko, P. Mai, E. Perepelitsky, and B. S. Shastry, *Phys. Rev. B* **96**, 054114 (2017); W. Ding, R. Žitko, and B. S. Shastry, *ibid.* **96**, 115153 (2017).
- [45] X. Deng, J. Mravlje, R. Žitko, M. Ferrero, G. Kotliar, and A. Georges, *Phys. Rev. Lett.* **110**, 086401 (2013).
- [46] J. Town *et al.*, *Comput. Sci. Eng.* **16**, 62 (2014).